Readout and Control of a Single Nuclear Spin with a Metastable Electron Spin Ancilla

Readout and control of a single nuclear spin with a meta-stable electron spin ancilla

Sang-Yun Lee[1+], Matthias Widmann[1], Torsten Rendler[1], Marcus W. Doherty[2]*, Thomas M. Babinec[3,4], Sen Yang[1], Moritz Eyer[1], Petr Siyushev[1], Birgit J. M. Hausmann[3], Marko Loncar[3], Zoltán Bodrog[5], Adam Gali[56], Neil B. Manson[2], Helmut Fedder[1+]*, Jörg Wrachtrup[1]

1. *3. Physikalisches Institut and Research Center SCOPE, University Stuttgart, Pfaffenwaldring 57, 70569 Stuttgart, Germany*
2. *Laser Physics Centre, Research School of Physics and Engineering, Australian National University, Canberra, A. C. T., 0200, Australia*
3. *School of Engineering and Applied Science, Harvard University, Cambridge, Massachusetts 02138, USA*
4. *Department of Applied Physics, Stanford University, 348 Via Pueblo Mall, Stanford, CA 9430 (current address)*
5. *Wigner Research Centre for Physics, Hungarian Academy of Sciences, PO. Box 1525, Budapest, Hungary*
6. *Department of Atomic Physics, Budapest University of Technology and Economics, Budafoki út 8, H-1111, Budapest, Hungary*

+These authors contributed equally

*e-mail: helmut.fedder@gmail.com

*e-mail: marcus.doherty@anu.edu.au

Electron and nuclear spins associated with point defects in insulators are promising systems for solid state quantum technology[1–3]. While the electron spin usually is used for readout and addressing, nuclear spins are exquisite quantum bits[4,5] and memory systems[3,6]. With these systems single-shot readout of single nuclear spins[5,7] as well as entanglement [4,8,9] aided by the electron spin has been shown. While the electron spin in this example is essential for readout it usually limits nuclear spin coherence[10]. This has set of the quest for defects with *spin-free* ground states[9,11]. Here, we isolate a hitherto unidentified defect in diamond and use it at room temperature to demonstrate optical spin polarization and readout with exceptionally high contrast (up to 45%), coherent manipulation of an individual excited triplet state spin, and coherent nuclear spin manipulation using the triplet electron spin as a meta-stable ancilla. By this we demonstrate nuclear magnetic resonance and Rabi oscillations of the uncoupled nuclear spin in the spin-free electronic ground state. Our study demonstrates that nuclei coupled to single metastable electron spins are useful quantum systems with long memory times despite electronic relaxation processes.

Coupled electron and nuclear spins in solids are promising candidates for quantum memories and registers and present a particular class in the emerging field of hybrid quantum systems[8,12–15], in which

different types of qubits perform distinct functions according to their advantageous properties. In this particular case, the nuclear spin, which is weakly coupled to the environment, serves as a long-lived quantum memory, whereas the electron spin, which has a short coherence time, but interacts strongly with external fields, serves as a readout gate[4,8,10]. In this architecture, the permanent presence of the electron spin is a source of decoherence to the nuclear spin[9]. To avoid such electron spin induced decoherence, the electron that carries the spin should be physically removed when it is not needed and returned to the nuclear spin only when the initialization or readout gate is applied. One approach to address this problem is to frequently remove the electron, e.g. by photo-ionization with a strong laser, resulting in a motional narrowing type of decoupling[10]. Another approach – that is followed in this work – is to choose an electronic system with a spin-free ground state and a meta-stable excited spin state that can be optically pumped and activated prior to the application of the readout gate[9]. Such a system implemented with a single solid state defect would enable a universal nuclear spin gate. In the following we present a suitable defect in diamond and demonstrate coherent control of a single nuclear spin in the spin-free electronic ground state. Notably, besides the NV center, this is the second known single spin defect in the solid state, whose coherent spin motion is detectable at room temperature.

The defect[1] is observed in ultra-pure single crystalline HPHT diamond after fabrication of vertical nano-wires (see Fig. 1a,b), whose main purpose is to provide high photon collection efficiency[16]. The wires are etched into the sample surface by reactive ion etching (see SI). Fig. 1c shows a confocal fluorescence microscope image of the sample. To identify candidates for meta-stable triplet spin defects, we observe the fluorescence intensity of bright spots on the sample surface with and without a strong applied magnetic field from a permanent magnet (≈0.5 T) (see Fig. 1d). An arbitrary oriented magnetic field causes spin mixing and thereby modifies the steady-state fluorescence[17]. We observe two types of emitters with decreasing and increasing fluorescence response, corresponding to NV^- centers and the new ST1 defects, respectively. The increase of the steady-state fluorescence is due to the mixing of meta-stable triplet states as will be shown later.

To characterize the defect further, we record the photon auto-correlation and observe a dip well below 0.5 at zero delay, which confirms that we indeed observe single defects[18] (see Fig. 1g). At higher excitation intensity, the photon auto-correlation shows pronounced 'bunching-shoulders', which supports the idea of the existence of a long-lived shelving state. To characterize the defect fluorescence, we present fluorescence emission spectra at room-temperature and at 10K (see Fig. 1e). In both cases a strong resonant emission line is observed at 550(1) nm, with a broad phonon side band extending to the near infrared. Notably, this resonant transition does not correspond to a known diamond defect line[19]. To characterize the strength of the optical transition, we present the excited state lifetime that we have determined in a room temperature experiment by pulsed optical excitation (see Fig. 1f). An excited state lifetime of 9.5(2) ns is observed.

Next, we search for a signature of an electron spin resonance in the optical fluorescence. Fig. 2a shows the fluorescence intensity that is observed while sweeping the microwaves from 200 to 1400 MHz. Three distinct lines marking an increase in fluorescence intensity upon spin resonance are observed at

[1] hereafter termed ST1-defect following the convention that is commonly applied in the EPR community

frequencies 2E = 278(1) MHz, D-E=996(1) MHz, D+E=1274(1) MHz. This optically detected magnetic resonance (ODMR) spectrum indicates a triplet electron spin with zero field splitting parameters[20] D=1135(1) MHz and E=139(1) MHz. The observed large E parameter could originate from the presence of a large local strain or from an intrinsic low symmetry of the defect. We have compared the spin resonance spectra of ~20 individual defects (see SI) and observed variations of the E parameter smaller than 5 MHz, indicating that the E originates from an intrinsic low symmetry of the defect. From ODMR spectra with a variable axial magnetic field applied (Fig. 2b), we determine an electronic g-factor $g_e = 2.0(1)$, close to the g-factor of the free electron spin. The absence of an intrinsic hyperfine splitting indicates that the defect's constituent atoms possess no nuclear spin (see SI for a detailed discussion of the possible constituents and structure of the defect). The aligned axial magnetic field has an angle of 35(1)° w.r.t the [111] crystal direction, indicating that the defect's main symmetry axis is oriented along the [110] crystal direction (see inset in Fig. 2b).

All findings reported up to here are compatible with two possible electronic configurations: the triplet state could either be the long lived shelving state or the ground state. To show that the triplet state is indeed the long lived shelving state, we measure the decay of the shelving state population. If the shelving state was a singlet, a single exponential decay would be expected. By contrast, in the present case, three distinct exponential decay terms are observed (Fig. 3b) and their amplitudes are sensitive to microwave fields resonant with the triplet ESR transitions. In each decay curve shown, the dominant decay terms are controlled by switching the spin population with microwave π-pulses resonant with the three ESR transitions. This indicates that the shelving state is indeed the triplet state. The result can be used to assign the decay constants to the spin quantum numbers (Fig. 3c). A complete model of the optical cycle can be established by determining also the triplet population rate by an analogous pulsed experiment (see SI). Fig. 3d summarizes all results related to the triplet kinetics. The essential features are: a rapid (~1/70 ns) inter-system-crossing rate from the singlet excited state to the triplet state and substantial differences among the triplet lifetimes, $\tau_{|0\rangle}$≈2500 ns, $\tau_{|-1\rangle}$≈1000 ns, $\tau_{|+1\rangle}$≈200 ns. These are responsible for the positive and exceptionally high (45 %) optical spin signal contrast, and increasing steady-state fluorescence response to a randomly aligned static magnetic field as observed in Fig. 1d because mixing the triplet sublevels results in faster decay to the ground state. It follows that optical pumping prepares the system in a spin polarized state of the meta-stable triplet state with predominant population of the slowly decaying triplet sublevel, $|0\rangle$. We now apply coherent spin manipulation to demonstrate Rabi oscillations between the triplet spin states (Fig. 4). Because the spin population of the faster decaying states $|+\rangle$ or $|-\rangle$ is increased by a resonant ESR pulse, any coherent spin manipulation results in the enhancement of the fluorescence intensity as shown in Fig.4b. The oscillations are described by two exponential decay functions, one of which is modulated by a cosine. The decay times and oscillation amplitudes correspond to the average of the lifetimes and the difference of the initial populations of the two involved spin states, respectively, and are in excellent agreement with the rates measured independently above (Fig. 3d). Note that the decay times are fully accounted for by the triplet lifetimes, which implies that spin relaxation is negligible. The triplet lifetimes are long enough to coherently address a coupled nuclear spin. We have compared the Zeeman sweeps of about 20 defects and observe that two of them show hyperfine splittings due to proximal $I = 1/2$ carbon nuclear spins of several tens of MHz see (Fig. 5a).

We now exploit the metastable electron spin for initialization and readout of the nuclear spin in the spin-free electronic ground state. To achieve this, we exploit the metastable electronic triplet spin ancilla to transfer spin-polarization onto and off the nuclear spin. To this end we exploit the optical nuclear polarization (ONP) induced by a level-anti-crossing (LAC) between the |-1,+1/2⟩ and |0,-1/2⟩ hyperfine levels at about 42 mT to selectively mix electronic and nuclear spin states[20,21] (see SI). Under these conditions, spin-polarization is transferred to the nuclear spin when the electron enters the meta-stable triplet level resulting in optical polarization of the nuclear spin[22]. After the optical pump pulse is turned off, the electron decays to the singlet ground state within a time given by the triplet lifetime. This decay eliminates the triplet electron spin and leaves the nuclear spin in its polarized state. Likewise, when the system is optically pumped from the singlet ground state to the excited triplet state, the nuclear spin state is preserved and the hyperfine levels are populated correspondingly. At the LAC, the different lifetimes of the hyperfine levels result in different fluorescent intensity of the nuclear spin projections. This provides a mechanism to readout the nuclear spin (see Fig. 5b and Methods). Fig. 5c shows the nuclear spin signal contrast as the energy levels are tuned into the LAC. Nuclear spin polarization is maximal at the LAC and vanishes when the detuning from the LAC becomes comparable to the hyperfine coupling strength. At the center of the LAC, the signal contrast is about 1.4 %. This observed contrast is slightly below the expectations from a 10-level rate model of the optical cycles that accounts for the mixed hyperfine levels and predicts a signal contrast of about 4 % and with the inversed sign. Given the observed ESR transition strengths at the LAC, we tentatively attribute this sign change to the readout contrast, however, a more detailed model is required to account for the precise ONP signal strength (see SI). As an application of the nuclear spin manipulation, we show nuclear magnetic resonance (NMR) and coherent manipulation of the nuclear spin via Rabi oscillations (Fig. 5 d,e). For the measurement of a nuclear magnetic resonance spectrum, we apply a radio-frequency (RF) π-pulse of variable frequency. We observe a resonance dip at 450(1) kHz, corresponding to the Larmor precession frequency $\nu_{13C} = \gamma_{13C} B = 447(5)\ \mathrm{kHz}$ of a bare ^{13}C nucleus. Here, $\gamma_{13C} = 10.705\ \mathrm{kHz/mT}$ is the gyromagnetic ratio of the ^{13}C nuclear spin and $B = 41.8(5)\ \mathrm{mT}$ is the applied field (corresponding to the LAC). We can thereby identify the coupled nuclear spin as a ^{13}C lattice spin. Note the absence of a chemical shift which indicates that indeed the electron spin is absent. For the measurement of nuclear Rabi oscillations, we apply a resonant RF pulse of variable length between the initialization and readout laser pulses. Several Rabi oscillations are observed that decay on a time scale of about 1 ms, which is an approximate measure of the nuclear T_2 time. The decay is likely to originate from dipole-dipole coupling of the nuclear spin to surrounding paramagnetic electronic defects and nuclear spin impurities. The time scale of the decay arising from coupling to the naturally abundant ^{13}C lattice spins can be estimated to be about 10 ms using observations of the T_2^* times of ^{13}C spin ensembles in diamond .[23] Note that in this case of a central ^{13}C spin, the coupling to the ^{13}C lattice spins is a spin diffusion mechanism. Given this estimate, coupling to electronic defects within the nano-wires, such as vacancy and interstitial related defects created by the large strain in the nano-wires, or surface defects and impurities are likely to account for the slightly faster decay observed. For future increase of the coherence time, the dipole interactions between the ^{13}C nuclei can be efficiently removed by homonuclear decoupling schemes[10,24–26] and interactions with paramagnetic electronic defects can be reduced by isolating ST1 defects in the bulk crystal.

The defect spin system presented in this work holds promise for room temperature solid state nuclear spin memories and quantum registers with ultra-long spin coherence times. Such a device could be used as a memory in integrated hybrid quantum systems[14,15] or as a solid state quantum token[10]. For such applications, coherence times on the order of seconds or hours are desirable. Owing to its spin-free ground state, the system presented here is a promising candidate for achieving such long coherence times by homonuclear dynamical decoupling, such as BLEW[24], FSLG[25], MREV[26]. An increase of the nuclear spin coherence time by several orders of magnitude is expected, as has been achieved recently with a single ^{13}C nuclear spin coupled to a single NV center[10].

Methods

Polarization and readout of the triplet spin state

A long intense laser pulse is applied to prepare the system in a spin-polarized state of the triplet level. The intensity and length of the pulse are chosen such that the optical transition is saturated and steady state fluorescence is reached during the pulse. Thereby the majority of the population is transferred to the slowly decaying triplet sublevel, while the two other triplet levels and the ground and excited states are nearly empty. The laser pulse is followed by a short idle time (~50 ns) to allow any residual population of the excited state to decay.

To readout the triplet spin state, the fluorescence is recorded during a laser pulse that is identical to the preparation pulse. Decaying fluorescence response curves are observed that encode the triplet populations. In particular, the fluorescence counts summed over a window at the beginning of the response profiles are proportional to the three triplet spin populations. This fluorescence is plotted in Fig. 3 and 4. In all data shown, a 200 ns integration window was used.

Polarization and readout of the nuclear spin

The nuclear spin is initialized by applying a long (10 μs) laser pulse (duration longer than several triplet lifetimes) followed by an idle time (20 μs) that ensures that the triplet population is fully decayed to the electronic ground state prior to any nuclear spin manipulation. The readout consists of a second laser pulse with simultaneous detection of the fluorescence, as in the case of the electron spin manipulation, except that now a longer (8 μs) integration window is used to accumulate fluorescence contrast. As before, the integrated fluorescence encodes the spin state.

Specification of measurement uncertainties

For the excited state lifetime, triplet state population- and decay rates, ESR resonance frequencies and line widths, electron- and nuclear spin Rabi oscillations and nuclear spin signal contrast, specified uncertainties are standard deviations of the model parameters (see text and figure captions for the respective model functions) obtained from maximum-likelihood estimation that originate from the poissonian distributed shot noise of the single photon counts (see SI for details on the multi-exponential fits). For the magnetic field calibration and g-factor of the ST1 electron spin, specified uncertainties are

standard deviations originating from the uncertainty of the magnetic field calibration via nearby NV-centers (see SI).

1. Ladd, T. D. *et al.* Quantum computers. *Nature* **464**, 45–53 (2010).

2. Koehl, W. F., Buckley, B. B., Heremans, F. J., Calusine, G. & Awschalom, D. D. Room temperature coherent control of defect spin qubits in silicon carbide. *Nature* **479**, 84–7 (2011).

3. Morton, J. J. L. *et al.* Solid-state quantum memory using the 31P nuclear spin. *Nature* **455**, 1085–1088 (2008).

4. Dutt, M. V. G. *et al.* Quantum register based on individual electronic and nuclear spin qubits in diamond. *Science* **316**, 1312–1316 (2007).

5. Neumann, P. *et al.* Single-shot readout of a single nuclear spin. *Science (New York, N.Y.)* **329**, 542–4 (2010).

6. Steger, M. *et al.* Quantum information storage for over 180 s using donor spins in a 28Si "semiconductor vacuum". *Science (New York, N.Y.)* **336**, 1280–3 (2012).

7. Pla, J. J. *et al.* High-fidelity readout and control of a nuclear spin qubit in silicon. 18 (2013).at <http://arxiv.org/abs/1302.0047>

8. Neumann, P. *et al.* Multipartite entanglement among single spins in diamond. *Science* **320**, 1326–1329 (2008).

9. Filidou, V. *et al.* Ultrafast entangling gates between nuclear spins using photoexcited triplet states. *Nature Phys.* **8**, 1–5 (2012).

10. Maurer, P. C. *et al.* Room-Temperature Quantum Bit Memory Exceeding One Second. *Science* **336**, 1283–1286 (2012).

11. Akhtar, W. *et al.* Coherent Storage of Photoexcited Triplet States Using ^{29}Si Nuclear Spins in Silicon. *Phys. Rev. Lett.* **108**, 1–5 (2012).

12. Brennecke, F., Ritter, S., Donner, T. & Esslinger, T. Cavity optomechanics with a Bose-Einstein condensate. *Science (New York, N.Y.)* **322**, 235–8 (2008).

13. Brown, K. R. *et al.* Coupled quantized mechanical oscillators. *Nature* **471**, 196–9 (2011).

14. Zhu, X. *et al.* Coherent coupling of a superconducting flux qubit to an electron spin ensemble in diamond. *Nature* **478**, 221–4 (2011).

15. Kubo, Y. *et al.* Strong Coupling of a Spin Ensemble to a Superconducting Resonator. *Phys. Rev. Lett.* **105**, 1–4 (2010).

16. Babinec, T. M. *et al.* A diamond nanowire single-photon source. *Nature Nanotech.* **5**, 195–9 (2010).

17. Epstein, R. J., Mendoza, F. M., Kato, Y. K. & Awschalom, D. D. Anisotropic interactions of a single spin and dark-spin spectroscopy in diamond. *Nature Phys.* **1**, 94–98 (2005).

18. Kurtsiefer, C., Mayer, S., Zarda, P. & Weinfurter, H. Stable solid-state source of single photons. *Physical review letters* **85**, 290–3 (2000).

19. Zaitsev, A. M. *Optical Properties of Diamond: A Data Handbook*. (Springer: Berlin, 2001).

20. Carrington, A. & McLachlan, A. D. *Introduction to magnetic resonance with applications to chemistry and chemical physics*. (Harper & Row: 1967).

21. Jacques, V. *et al.* Dynamic Polarization of Single Nuclear Spins by Optical Pumping of Nitrogen-Vacancy Color Centers in Diamond at Room Temperature. *Phys. Rev. Lett.* **102**, 7–10 (2009).

22. Colpa, J. P. & Stehlik, D. Optical nuclear polarization as a consequence of the non-crossing rule (level-anti-crossing). *Chemical Physics* **21**, 273–288 (1977).

23. Hoch, M. & Reynhardt, E. Nuclear spin-lattice relaxation of dilute spins in semiconducting diamond. *Phys. Rev. B* **37**, 9222–9226 (1988).

24. Burum, D. ., Linder, M. & Ernst, R. . Low-power multipulse line narrowing in solid-state NMR. *Journal of Magnetic Resonance (1969)* **44**, 173–188 (1981).

25. Bielecki, A., Kolbert, A. C. & Levitt, M. H. Frequency-switched pulse sequences: Homonuclear decoupling and dilute spin NMR in solids. *Chemical Physics Letters* **155**, 341–346 (1989).

26. Rhim, W.-K. Enhanced resolution for solid state NMR. *The Journal of Chemical Physics* **58**, 1772 (1973).

Acknowledgements

We acknowledge support by the DFG via Forschergruppe 1493 and SFB/TR21 as well as the EU via the ERC grant SQUTEC and FP7 grants DIAMANT and QINVC. B.H. gratefully acknowledges support from HQOC. We thank Matthew Sellars, Phil Hemmer, Philipp Neumann, Roman Kolesov, Rainer Stöhr and Christian Burk for fruitful discussion.

Author contributions

S.L., H.F., and J.W. designed the experiments. S.L., M.W., T.R., T.B., S.Y., M.E., P.S., and H.F., performed the experiments. S.L., M.W., M.D., and H.F. analyzed the data. B.H. and M.L. fabricated the nanopillars.

M.D., Z.B., A.G., and N.M. provided the theoretical support. Everyone discussed the data and commented on the manuscript. S.L., M.D., H.F., and J.W. wrote the paper.

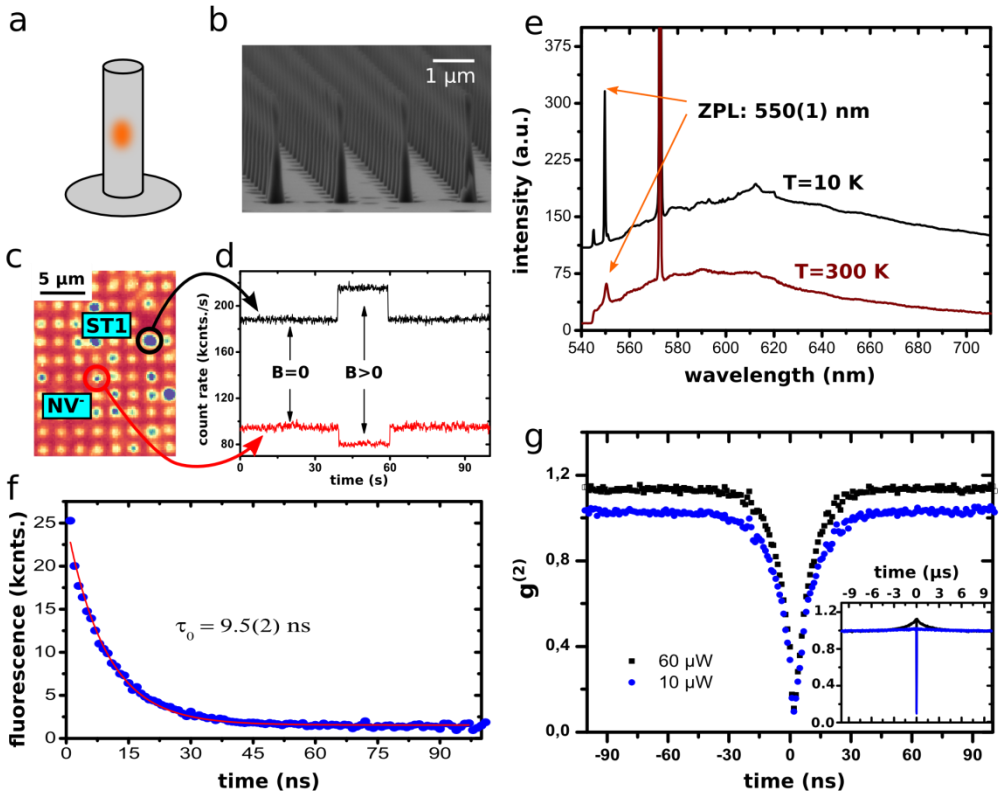

Fig. 1| Optical properties of the ST1 defect. a, Illustration of a diamond nano wire containing a single fluorescent point defect. **b,** SEM image of the [111] HPHT diamond sample with fabricated nano wires (diameter ~200 nm, length ~2 µm). **c,** confocal fluorescence microscope image of the sample. The marked wires contain single NV^- and ST1 defects. **d,** fluorescence time trace recorded during application and removal of a non-aligned magnetic field. The fluorescence is quenched and enhanced for NV-, and ST1 defects, respectively. **e,** fluorescence emission spectrum of a single ST1 defect at room temperature and liquid helium temperature. A zero phonon line at 550(1) nm and a broad emission band in the red to NIR range is observed. The sharp peak at 573 nm is due to inelastic Raman scattering of the 532 nm excitation laser, **f,** fluorescence decay showing an excited state life time of 9.5 ns, **g,** second order photon correlation at increasing excitation power. The dip at delay t=0 reaches well below 0.5, proving the single center nature of the defect. At high excitation power pronounced bunching shoulders are observed, that indicate the presence of a long lived shelving state.

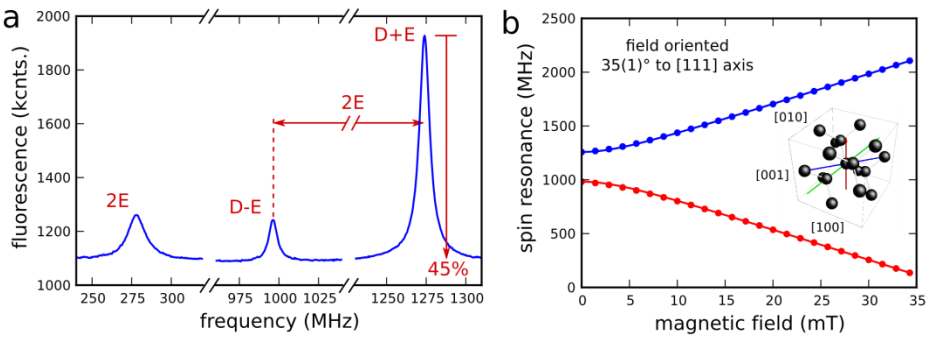

Fig. 2| Optically detected electron spin resonance. a, room temperature ESR spectrum at zero magnetic field. Resonant transitions are indicated by their zero-field splitting parameters D=1135(1) MHz and E=139(1) MHz. We observe an exceptionally high optical spin signal contrast of the D+E spin projection of about 45 %, **b,** Zeeman curve with an aligned axial magnetic field oriented along the defect main symmetry axis (35(1)° w.r.t. the [111] crystal axis); dots: experiment, lines: theoretical fit obtained from the triplet spin Hamiltonian $H = D\left[{S_z}^2 - S(S+1)/3\right] + E\left({S_x}^2 - {S_y}^2\right) + gS_zB_z$, where S_α are the usual spin operators for total Spin $S = 1$, g is the g -factor and B_z is the axial field (see SI). The inset shows a schematic illustration of the crystallographic orientation of the defect. Green, blue and red arrows denote the [111], [110] (defect's main axis) and [001] (C_{2v} symmetry axis), respectively.

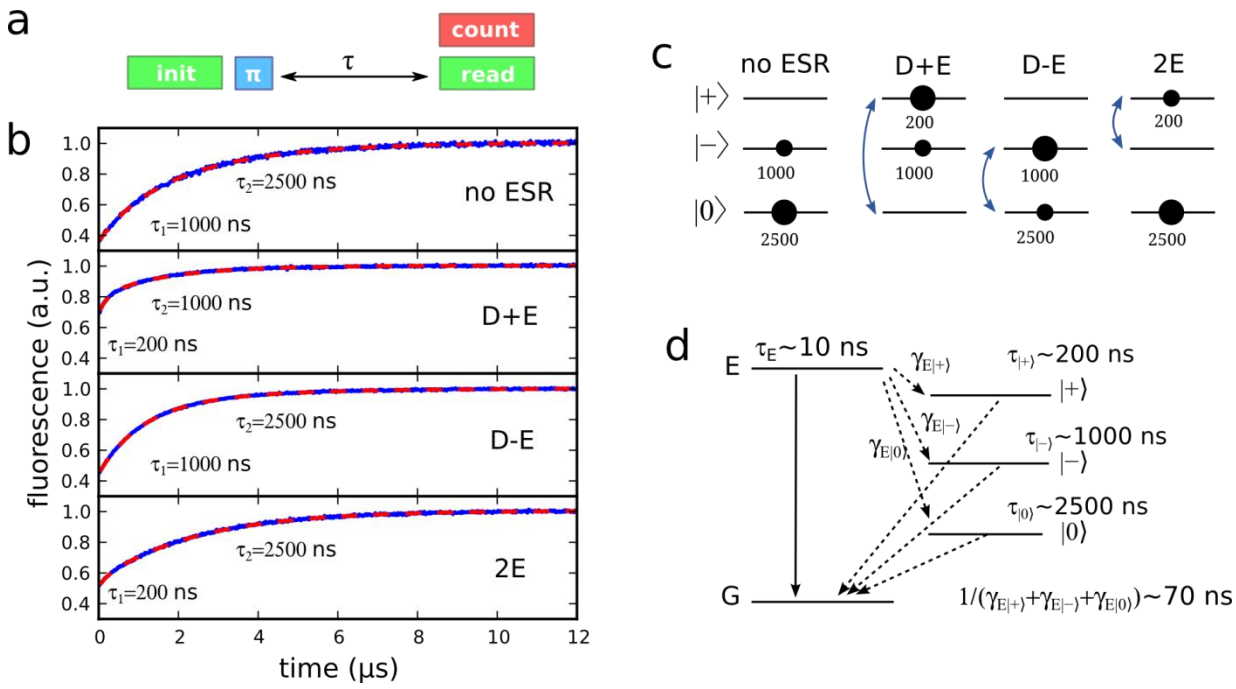

Fig. 3| Kinetics of the shelving state and energy level scheme at zero magnetic field. a, optical and microwave pulse sequence for the measurement of the shelving state lifetimes. After an optical pump pulse, a resonant microwave π-pulse is applied to exchange the populations of selected spin sublevels and thereby control the dominant decay constants, **b,** Decay curves of the shelving state population described by double exponential functions $y = c - a_1 \exp(-t/\tau_1) - a_2 \exp(-t/\tau_2)$. Blue: experimental data, red dashes: double exponential fits (see SI). For each panel, the microwave π-pulse is resonant with the denoted ESR transition, **c,** Assignment of the decay constants to the triplet energy levels. The initial populations (no ESR), are proportional to the decay constants. The small population of the short lived state is omitted. The observed decay constants imply the assignment of the energy levels denoted on the left, **d,** Summary of the triplet kinetics and electronic structure consisting of singlet ground- and excited states and a meta-stable triplet state. Transition rates between two states i and j

and the lifetime of a state i are denoted γ_{ij} and τ_i, respectively.

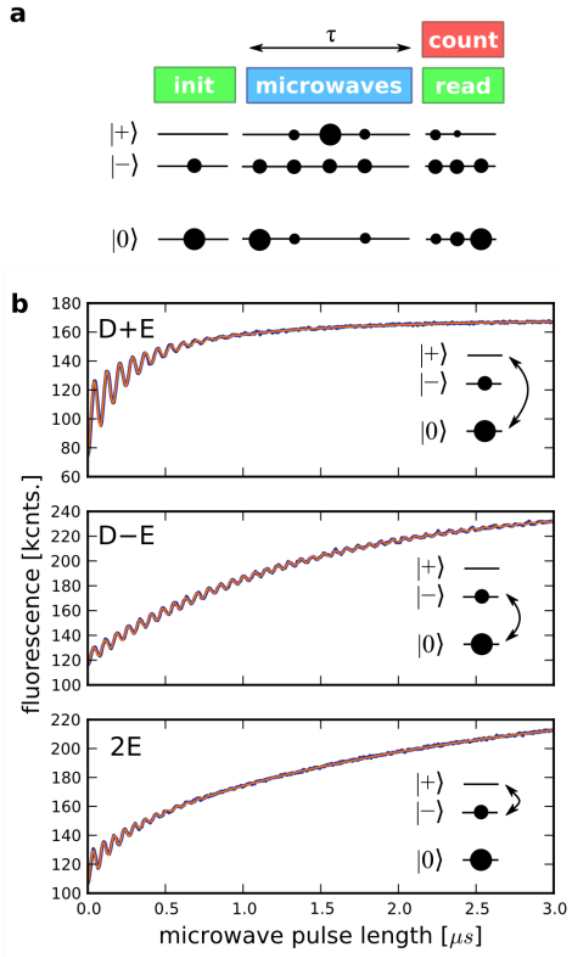

Fig. 4| Coherent triplet spin manipulation. a, Optical and microwave pulse sequence and evolution of the triplet populations (here illustrated for microwaves resonant with the D+E transition), **b,** Rabi oscillations among the triplet spin sublevels at zero magnetic field. Thick blue lines show experimental data, thin red lines show theoretical fits with the model $I = I_0 - (a_1 + a_2 \cos \Omega t) \exp(-t/\bar{\tau}) - a_3 \exp(t/\tau)$, where $\bar{\tau} = 2({\tau_\alpha}^{-1} + {\tau_\beta}^{-1})^{-1}$ is a combined decay constant of the levels α and β involved in the Rabi oscillations, τ is the decay constant of the remaining level, a_i are fluorescence amplitudes and Ω is the Rabi frequency. Note that for the upper and lower panel the combined decay constant is dominated by the fast decay of the $|+\rangle$ level. For the fit shown in the middle panel the last term is omitted, since the unaffected level is the $|+\rangle$ level, which (nearly) unpopulated.

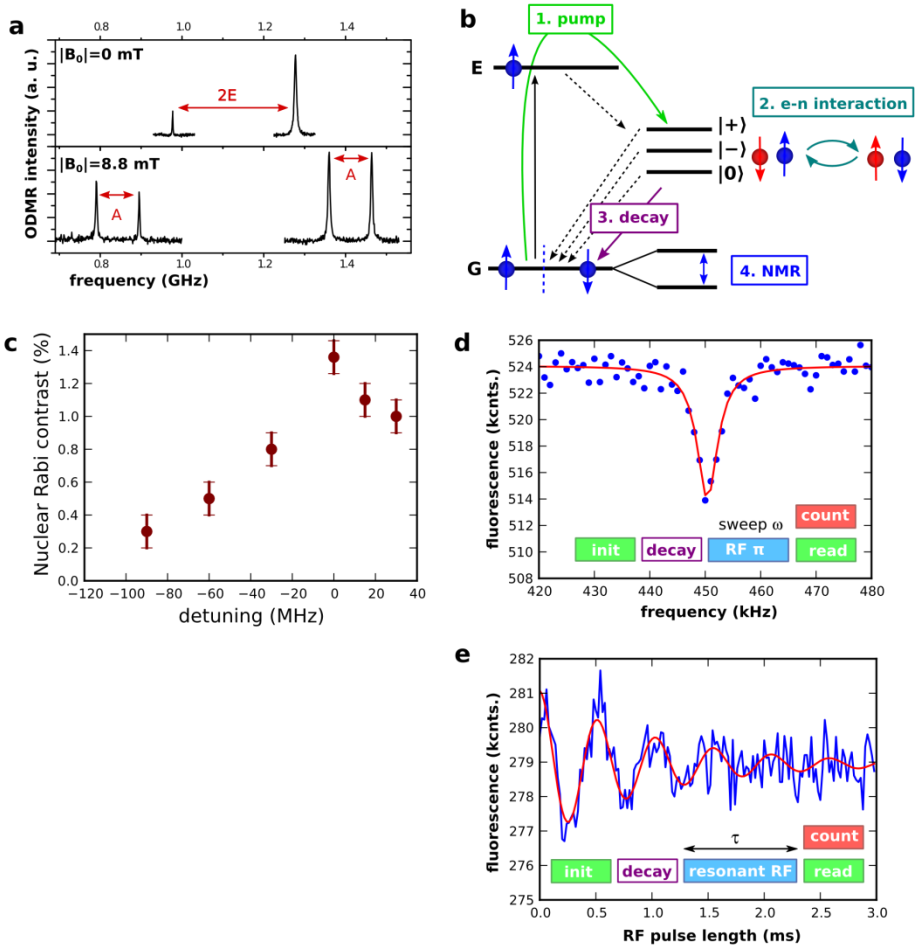

Fig. 5 | **Readout and control of a single nuclear spin in the spin-free electronic ground state. a,** ODMR spectra of an ST1 defect with a nearby ^{13}C nuclear spin, under zero (upper panel) and moderate (lower panel) magnetic field applied along the defect's axis. E and A denote the zero-field- and hyperfine-splitting parameters, respectively. The hyperfine splitting is suppressed at small fields and becomes visible when the Zeeman energy is larger than the E parameter. **b,** Readout and control of the nuclear spin with the electronic triplet spin ancilla. The nuclear spin (blue arrows) is interrogated by optically pumping the electron spin (red arrows) into the triplet state and allowing the electron and nuclear spin to interact. The subsequent decay of the triplet state destroys the electron spin and leaves the nuclear spin unchanged. The bare nuclear spin is then coherently manipulated by NMR. Efficient transfer of spin polarization between the electron and nuclear spin in the triplet state is provided by exploiting an ONP as a consequence of LAC between the |-1,+1/2⟩ and |0,-1/2⟩ hyperfine levels (see text), **c,** Signal contrast of nuclear Rabi oscillations, corresponding to the product of the nuclear spin polarization and readout contrast, as a function of detuning from the LAC (zero detuning corresponds to the LAC). **d,e,** NMR spectrum and Rabi oscillations of the nuclear spin in the electronic ground state. For the NMR spectrum (d), an RF π-pulse of variable frequency is inserted between the preparation and readout laser pulses. The resonance dip corresponds to the Larmor precession of a bare ^{13}C nuclear spin. Blue: experimental data, Red: Lorentzian fit. Note that the NMR line width (4.5(2) kHz obtained from the

Lorentzian fit) is determined by power broadening and in the present case of a pulsed measurement corresponds approximately to the inverse RF π-pulse width (0.2 ms). For the Rabi oscillations (e) a resonant RF pulse of variable length is inserted between the initialization and readout laser pulses. Blue: experimental data, red: exponentially decaying cosine fit; decay constant 1.0(1) ms.